Detailed Magnetic Field Monitoring of Short Circuit Defects of Excitation Winding in Hydro-generator

H. Ehya, *Student Member, IEEE*, A. Nysveen, *Senior, IEEE*, I. L. Groth, and B. A. Mork, *Senior, IEEE*

***Abstract*—The excitation windings of the synchronous generators are generally reliable. However, electrical, mechanical, and thermal stresses that the machine is exposed to during its operation leads to the inter-turn and ground insulation faults. On-line condition monitoring could provide a valuable real-time assessment of the synchronous generator. It could discriminate gradual aggravating defects at an incipient stage before it leads to irreversible and costly damages. On-line monitoring of the air gap magnetic field has been used in different types of electrical machines. However, some concerns should be considered when applying this method to the salient pole synchronous generators (SPSG), especially in the SPSG, with a large number of turns per poles that show less or lack of sensitivity to a fault. This difficulty could be solved by wise locating of the Hall effect sensor, choosing precise sampling rate, re-sampling the data and signal processing approach. In this paper, detailed online monitoring of the air gap magnetic field under the excitation winding defect is proposed. A procedure that could detect the severity and location of the fault-based on different analyzing methods of flux density in no-load and full load is proposed. The nominated approach is examined by using numerical modeling and a experimental test rig with a 100 kVA SPSG. It is proven that the air gap magnetic field spectrum could provide a reliable assessment of the machine under the short circuit fault of the rotor field winding.**

***Index Terms*—Air-gap magnetic field, condition monitoring, hall effect sensor, hydro-generators, re-sampling, short circuit defect.**

I. Introduction

Salient pole synchronous generators are the most commonly used machine in hydropower plants. The hydropower generators are subjected to a wide range of electromagnetic and mechanical disturbances, abnormal operating conditions, which results in different kinds of faults. Generally, hydropower plants have a sophisticated protection system that consists of over-voltage, over-current, differential relays in addition to several subsystems and equipment that trip automatically as a quick response to abnormal operating conditions. The purpose of the protection system is to ensure immediate and correct disconnection of the production unit in the event of a severe fault in the machine or the power network that is connected to.

The incipient faults like the inter-turn short circuit of the excitation winding, eccentricity, and broken damper bar cause non-ideal operating conditions and may aggravate with the time. However, they do not impose any immediate hazards to the generator and leads to outsourcing it. Detection of these defects is difficult, especially at its early stage, since they do not impose significant changes to the overall operation of the synchronous generators [1]. Besides, these defects may exist for a long time unnoticed by the protection system.

The incipient fault diagnostic could prevent future severe damages to the synchronous generators. The traditional approach, like a visual inspection for abnormalities like discolorations or fractures as well as off-line tests, are commonly used for the incipient fault detection of the synchronous generators. The off-line condition monitoring has some drawbacks since the synchronous generator is shouted down. In addition, it requires some additional resources to perform the test, and disassembly of the generator component to do measurement is the additional problem. In some cases, defects happen between the scheduled condition assessment period and result in severe damages to the machine. Furthermore, some kind of faults is disappeared due to the absent impact of centrifugal forces in the stand-still measurement of the offline test [2] [3]. Therefore, online condition monitoring of the synchronous generators is the practical solution to overcome the difficulties related to the off-line test.

The search coils mounted in the air gap of the cylindrical synchronous generator has become a well-established concept for online condition monitoring [4]. The fault detection based on magnetic flux density is an invasive method. However, it is a critical parameter that could reveal various faulty states of the machine [5]. Several magnetic monitoring methods and sensors had been developed for a cylindrical rotor synchronous generator, but that approach is not proper for fault detection of SPSG. The concentrated field winding, the saliency of the poles, and a large number of pole pairs entail a more sophisticated analysis when investigating the magnetic field distribution compared to cylindrical-rotor synchronous generators [6]. The induced voltage in the search coil that is installed in the stator slots of SPSG is used to detect short circuit fault in the rotor winding. The peak amplitude of the induced voltage is compared to the nearby pole that sweeps through the search coil.

This work was supported by Norwegian Hydropower Centre (NVKS) and Norwegian Research Centre for Hydropower Technology (HydroCen).

Hossein Ehya, Arne Nysveen are with the Department of Electrical Power Engineering, Norwegian University of Science and Technology (NTNU), 7034 Trondheim, Norway. (e-mail: hossein.ehya@ntnu.no) Ingrid Linnea Groth is with Siemens, Trondheim, Norway. B. A. Mork is with Department of Electrical and Computer Engineering, Michigan Tech University, United States.

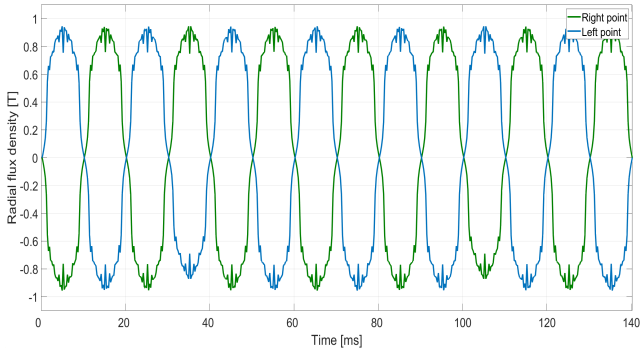

Fig. 1. The air gap magnetic filed in no-load under 7 turns short circuit fault - Simulation result.

TABLE I
100 kVA, 400 V, 14 POLES, 428 RPM, 50 Hz, SALIENT POLE SYNCHRONOUS GENERATOR

Quantity	***Values***	***Quantity***	***Values***
No. of slots	114	No. of damper bars/pole	7
Stator outer diameter	$780mm$	Stator inner diameter	$650mm$
Widths of stator tooth	$8.5mm$	Height of stator tooth	$29.5mm$
Widths of pole shoe	$108mm$	Widths of pole body	$50mm$
Length of stack	$208mm$	Minimum air gap length	$1.75mm$
No. of stator turns	8	No. of rotor turns / pole	35

However, the peak value of the signal is not a reliable index for fault detection since the failure in neighboring pole could significantly influence the amplitude of the healthy pole as well.

This paper includes a detailed electromagnetic analysis of the SPSG in a healthy and incipient inter-turn short circuit fault using the FE method. A procedure for short circuit defects in an excitation winding is proposed based on the average radial flux, polar diagram, sum of two sensors flux density, and frequency spectrum monitoring. The effects of the sensor location, sampling frequency, and re-sampling of the data are studied. Load effects on proposed methods are studied. The simulation results are verified by results of the 100 kVA custom-made SPSG in the laboratory.

II. ELECTROMAGNETIC ANALYSIS

A reliable fault diagnosis is based on a precise modeling method. The time-stepping finite element method is employed to simulate SPSG. In this modeling, detailed geometrical complexities of the machine, such as stator slots and rotor damper bars, are considered. In addition, the saliency of the rotor poles, the spatial distribution of armature winding, non-linearity of the core materials are included. The specifications of the proposed SPSG have been summarized in Table I.

The total magneto-motive force of the faulty pole under the inter-turn short circuit fault is reduced. Consequently, the flux density of the effected pole is decreased, and the air gap magnetic field is distorted. Two Hall effect sensors are located on two separate stator teeth opposite each other to measure the air gap radial magnetic field (these two sensors are named as of right and left point). The modeled SPSG has 14 poles that each pole has 35 turns. Different degrees

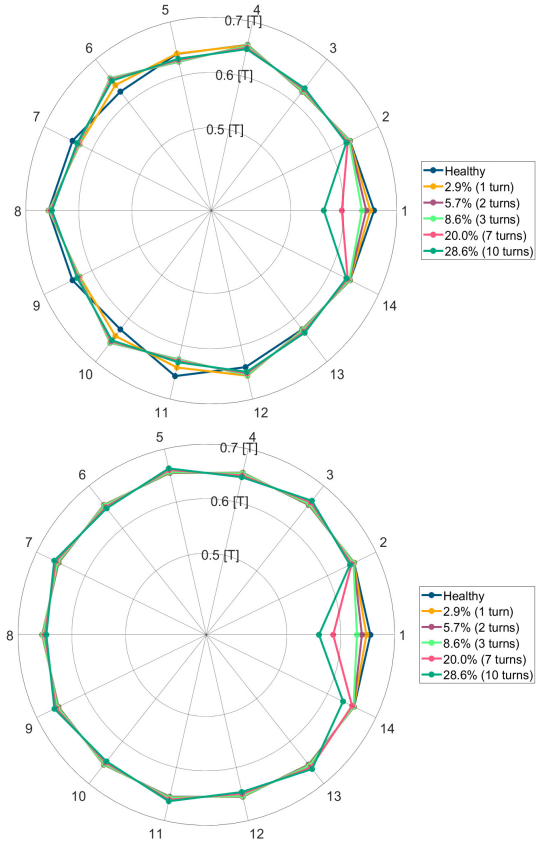

Fig. 2. Polar diagram of the average flux density of the each pole under short circuit fault in no-load (top), maximum load (bottom) - Simulation result.

of inter-turn short circuit fault with the severity from 1 to 10 turns is simulated.

Fig. 1 depicts the air gap magnetic field variation for a one full rotor revolution that 7 out of 35 turns are short-circuited in one pole. The flux density in the air gap has a lower amplitude when the faulty pole sweeps by the sensors in comparison to healthy poles since the faulty pole with the reduced ampere-turns produces a decreased magneto-motive force. Inter-turn short circuit fault diagnosis is possible by comparing the average flux density of each pole to each other. However, fault detection is difficult in a case the number of shorted turns or the percentage of the shorted turns to a total number of pole turns is low.

An average flux density of each pole in the space as a polar diagram for a healthy and faulty synchronous generator simulated in FEM is shown in Fig. 2. In a healthy and ideal machine, the radial distance from the origin of a polar diagram to the average value of each pole would be equal. The average value of the rotor pole magnetic field decrease by increasing the number of short-circuited turns. The average flux density of the faulty pole with respect to the average flux density of the all poles with 1, 2, 3, 7, and 10 short circuit turns are 99%, 97.9%, 96.8%, 93.7%, and 88.8%, respectively. The average flux density of the faulty pole is also decreased in full load case as shown in Fig. 2 (bottom).

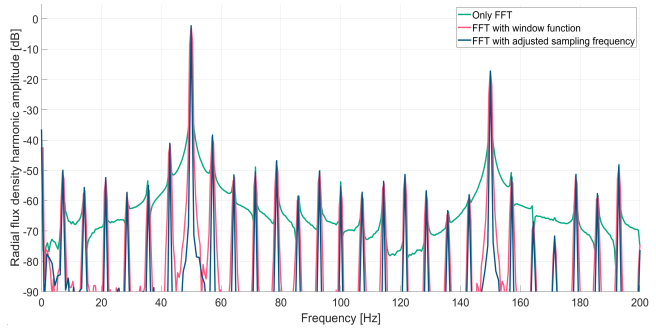

Fig. 3. The comparison of the spectrum density of the magnetic field by using FFT function, Hann window, and the adjusted sampling frequency.

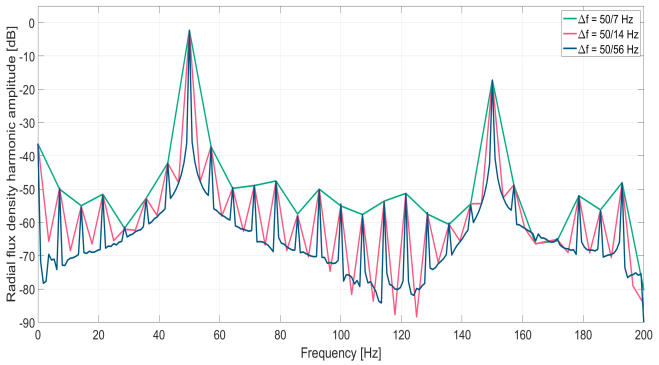

Fig. 4. The impact of the frequency spacing on spectrum density of the magnetic field.

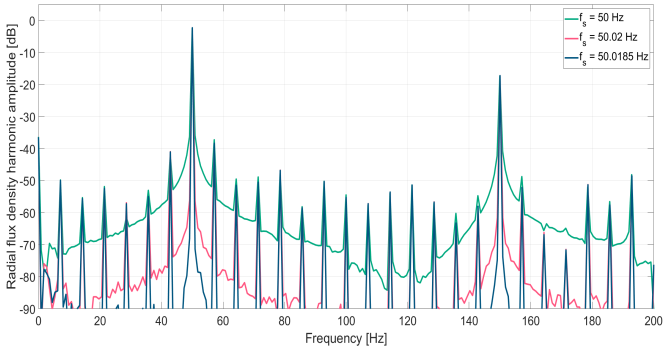

Fig. 5. The impact of fundamental frequency spacing on spectrum density of the magnetic field.

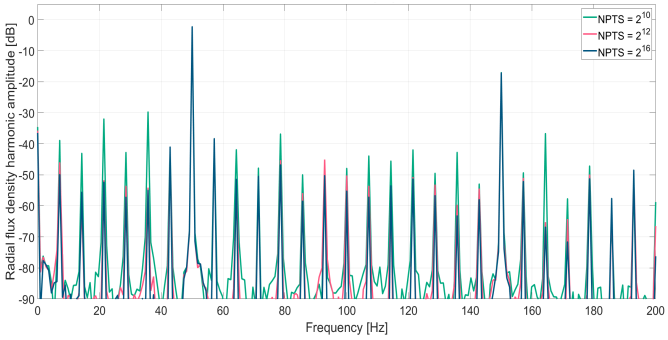

Fig. 6. The impact of the NPTS on the spectrum density of the magnetic field.

The average flux density in the presence of 1, 2, 3, 7 and 10 short circuit turns reduced to 99%, 97.9%, 96.7%, 90.7%, and 87.3%, respectively.

III. Advanced Signal Processing

Fast Fourier transform is an advantageous processing tool to get the precise spectrum density of the signal. In comparison to many signal processing tools that could detect the chaos in the signal, computational time of the FFT make it proper and applicable tool especially for real time analysis. However, there are some criteria that should take into account when utilizing the FFT approach as below:

1) The length of the input data processed by the FFT function can be adjusted to the expected output.
2) The sampling frequency can be adjusted to increase the frequency resolution of the output.

In order to meet above properties, the sampling frequency is chosen as follow [7]:

$$\triangle f = \frac{1}{NPTS * \triangle t} \tag{1}$$

where $\triangle f$ is the frequency spacing of the FFT, $NPTS$ is the number of sampled points to be transferred to the FFT and $\triangle t$ is the inverse of the sampling frequency. This method works very well when the expected frequency components are predictable.

In order to achieve the accurate spectrum density results, the frequency spacing $\triangle f$ must be chosen such that $\triangle f$ and its integer multiplum should be coincide exactly with the fundamental frequency and its sub-harmonics. Besides, $NPTS$ must be an even integer. Fig. 3 depicts the result of frequency spectrum by applying FFT algorithm, Hann windowing function before the FFT function and the adjusted sampling frequency before the FFT function. The two first approaches resulted in distributed spectra because the length of the data set did not correspond to a complete number of periods and leads into magnitude errors and side-lobe distortion. A discrete and clear line spectra where the harmonics hit the corrects frequencies and showed more consistent amplitudes are achievable by utilizing the adjusted sampling frequency based on Eq. 1.

There are only a few standard sampling frequency rates in the data acquisition systems that could not conformed with the required sampling frequency as in Eq. 1. Therefore, the sampled data set must be re-sampled by using cubic spline interpolation function.

Fig. 4 shows the impact of changing the spacing frequency while $\triangle t$ depends on the given value of the $\triangle f$ ($NPTS$ is assumed to be constant value). The value of the $\triangle f$ and its integer multipliers must be chosen in way that pop up on the expected frequency of the spectrum as stated above. For a machine with 7 pole pairs, the smallest frequency component is equal to 7.14 Hz for a 50 Hz power frequency which is the same as the mechanical frequency

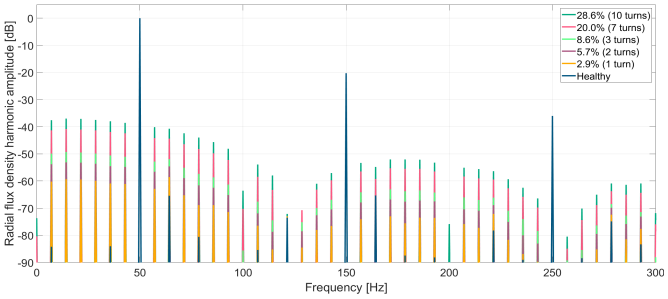

Fig. 7. Spectrum density of the radial flux under short circuit fault in no-load - Simulation result.

of the machine. Consequently, the denominator has to be integer multiples of 7 in order to hit the correct frequencies in the spectrum. The amplitudes of each frequency component have the correct values for spacing frequency equal to $50/7$, however the spectrum "floats together" which makes it hard to determine where each frequency component actually is. Decreasing the spacing frequency to half and seventh of its original value improves the spectra quality. The spikes at each frequency component becomes more narrow when decreasing $\triangle f$ and the curve between each frequency component descends. The amplitudes of the frequency components in all three cases however trace virtually the exact same values.

The length of the data set determines the lower limit of $\triangle f$. In Fig. 3, the original data set consists of 100,000 data points sampled at a rate of 50 kHz. Thus, the total length of the measured data is equal to 2 seconds (100,000 points/50 kHz). If the inverse of $\triangle f$ exceeded the length of the sampled data, the spline interpolation became unstable and approached infinity. The reason is that the period of the inverse of $\triangle f$ can not exceed the total length of the signal. This implies that in order to decrease $\triangle f$, the length of the measurement must be increased.

Choosing a small spacing frequency such that $\triangle f$ and every integer multiple of that would coincide with the expected frequency components of the spectrum was sufficient when applying the FFT algorithm to the simulation results, but it is not applicable for the measured data set obtained from the experimental test rig. The reason is that the speed deviated somewhat from rated speed and the fundamental frequency of the field test generator is not exactly 50 Hz. In fact, the frequency of grid connected hydropower generators always differs slightly from 50 Hz, thus an algorithm that takes this into consideration is required. Fig. 4. shows the effect of adjusting the fundamental frequency before performing the spline interpolation and the FFT. Tuning the fundamental frequency resulted in more defined peaks and concentrated lines in the spectra and the curve between each frequency component fell below -90 dB for the most part of the spectrum. The amplitudes of the frequency components in Fig. 4 varies depending on the specified fundamental frequency. The largest deviation between the 50 Hz spectrum and the corresponding frequency component of the 50.0185 Hz spectrum was about 3.5 dB.

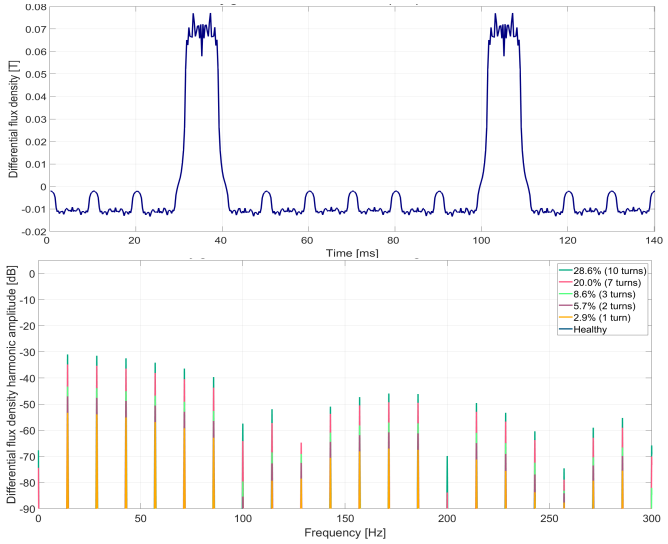

Fig. 8. The differential magnetic field of the air gap under 7 turns short circuit fault at no-load (top), the spectrum density of the above signal (bottom).

Fig. 5 depicts the influence of changing the number of sampled points ($NPTS$) on the spectrum density. The spacing frequency is kept constant at 50.0185/56 Hz, while $\triangle t$ depends on the given value of $NPTS$ according to Eq. 1. It was found that when the new sampling rate approached the original sampling rate by increasing the $NPTS$, the change in amplitude of the frequency components diminished. The amplitudes of the frequency components stopped changing and stabilized by increasing the value of the $NPTS$ further such that the new sampling frequency exceeded the original sampling frequency.For data sets containing 100,000 points sampled at 50 kHz for instance, $NPTS$ was set to 2^{16} or higher.

The differences between the three spectra obtained with different sampling frequencies (10, 25, and 50 kHz) were marginal. The spike at each frequency component gets slimmer or more concentrated with decreasing sampling frequency. The reason for this is that the measurements contain more cycles, which increases the frequency resolution of the spectrum by allowing for a smaller $\triangle f$ to be applied. However, the variation in amplitude of the three spectra are less than 0.5 dB. It was thus concluded that the original sampling frequency had little impact on the final frequency results and that all the three listed sampling frequencies would work well for the purpose of the frequency analysis.

IV. Signal Processing

The frequency spectrum of the air gap magnetic field in Fig. 7 shows significant changes in the side-band harmonics as a result of the inter-turn short circuit fault in the excitation winding. The amplitude of the fault-related harmonics increased with the increasing number of shorted turns. The index frequency identifier is as follows:

$$f_{fault} = f_s \pm k f_r \tag{2}$$

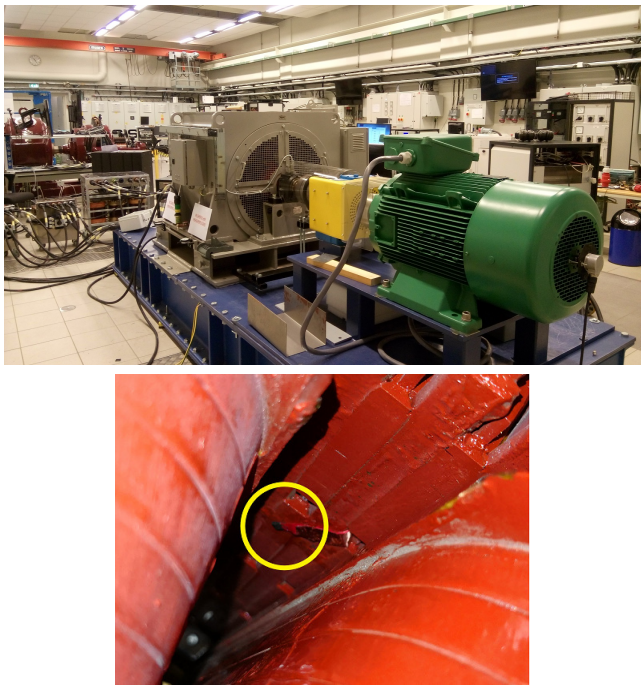

Fig. 9. The experimental test rig of a 100 kVA synchronous generator. The location of the hall-effect sensor installed on stator tooth

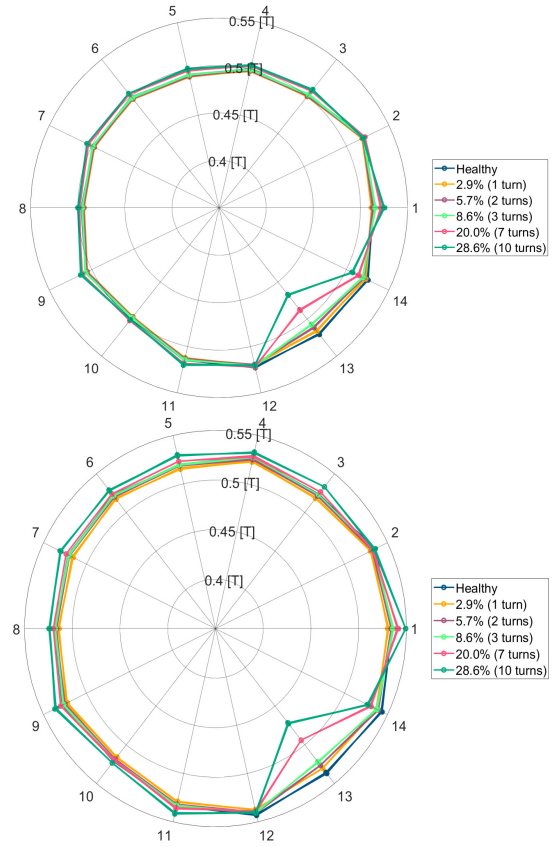

Fig. 10. Polar diagram of the average flux density of the each pole under short circuit fault in no-load (top), maximum load (bottom) - Experimental result.

where f_s is the electrical frequency, f_r is the mechanical frequency of the rotor, and k is an integer. The most significant fault-related harmonic component in the frequency spectrum appears at the frequencies below the fundamental harmonic as seen in Fig. 7. The amplitude of the 7.14 Hz component with one short-circuited turn is about -60.22 dB or about 1 mT. With two short-circuited turns, the amplitude increases to about to 2 mT, and with 10 turns, the amplitude is about 10.3 mT. The magnitude of all the fault-related harmonics shows a more or less linear increase in amplitude with increasing numbers of short-circuited turns.

The frequency spectrum of the sum of the magnetic field of two installed hall effect sensors in the air gap could also reveal the machine condition state. In a healthy and balanced operating condition, the two sensors based on theory are experiencing an identical variation in flux density, causing the summation of them to become zero. In the event of short-circuited turns in the field winding, the reduced flux density of the faulty pole causes increased (Fig. 8) value of side-band in the sum of flux density each time the faulty pole passes by one of the measuring points. The simulation results of the healthy synchronous generator show that the fundamental component and its odd multiples are effectively canceled out in the frequency spectrum (Fig. 8). The frequency components appear in the frequency spectrum are a direct consequence of the short-circuited turns in the field winding, which distorts the inherent magnetic symmetry of the healthy machine. In addition, there are fewer fault-related harmonics in the frequency spectrum. This spectrum only contains frequency spectra of Eq. 2 at odd multiples of the k. The amplitude of the sum of the magnetic field spectrum is higher than the radial magnetic flux spectrum that makes fault detection easier.

V. Experimental Verification

A 100 kVA salient pole synchronous generator is used to verify the proposed theory (Fig. 9). Apart from its size, the topology of the generator resembles an actual hydropower generator in the Norwegian hydropower plants. The laboratory SPSG has 14 poles, and the length of the air gap is 1.75 mm in order to achieve the proper synchronous reactance. The main components of the experimental set-up are explained as below:

1) A 90 kW induction motor is used as a prime over at the rated speed of 1482 rpm.
2) Induction motor's shaft is connected to the synchronous generator by using a gearbox.
3) A DC power SM3300 DELTA ELEKTRONIKA is used to magnetize the field winding.
4) An external rectifier is used to supply the programmable converter which is used to run the induction motor.
5) The hall-effect sensors (AST244) with a dimension of $(3.0 \times 5.0 \times 0.8) mm$ is glued on the stator tooth. The ratio of the induced voltage to the magnetic field

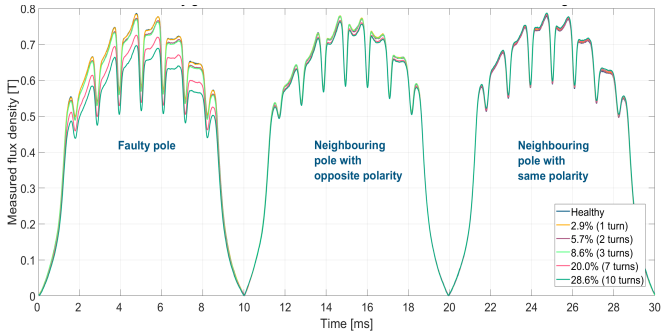

Fig. 11. Radial flux density of the faulty pole and its neighboring poles under short circuit fault at no-load - Experimental result.

is 2.54 T/V. A constant DC power supply with an approximate current equal to 4.75 mA is used to feed the sensor.

6) A high-resolution oscilloscope (16-bit) is used for data acquisition with a sampling frequency of 20 kHz
7) In order to avoid the harmonic interference from the network a set of passive load which consists of resistive and inductive load with different configuration is used to load the synchronous generator.

Fig. 10 shows the average value of the magnetic field for each pole as a polar diagram in the presence of rotor field winding short circuit fault. It depicts how the flux density of the faulty pole and also the healthy poles were affected by the short-circuits applied to the field winding. For minor fault severities, the change in average value is marginal. The effect of 7 or 10 short-circuited turns on the other hand is evident. The center of the average value of magnetic field diagram does not coincide with the center of polar diagram by comparison of Fig. 10 to Fig. 2. The movement of the center in the measurement results is due to the inherent dynamic eccentricity fault. Imposing the effects of the short-circuited turns in pole 6 and the dynamic eccentricity together at the same time, these two effects will reinforce one another, possibly causing the dynamic eccentricity to further intensify.

The absolute value of the flux density of the faulty pole and the two posterior poles passing by the right sensor are shown in Fig. 11. The faulty pole responds as expected; the flux density decreases with an increasing number of shorted turns. The flux density of the neighboring pole with opposite polarity is also decreased slightly with an increasing number of short-circuited turns. This is a result of the decreased flux following the path throughout the faulty pole and on to the adjacent poles of opposite polarity.

Table II shows the percentage reduction in average value of faulty pole with respect to the average value of all the poles during healthy operation and for the various numbers of short-circuited turns in no load and three loading scenario.

The three load cases listed in Table II in addition to no-load case where load-1 is low resistive load (30 kW, power factor (PF) 1), load-2 is low resistive/inductive load (40 kW - PF 0.79) and load-3 is high resistive/inductive load (65 kW - PF 0.93). The average value of pole 6 is not 100% during

TABLE II
THE AVERAGE VALUE OF MAGNETIC FIELD IN A PRESENCE OF SHORT CIRCUIT FAULT IN ROTOR FIELD WINDING COMPARED TO NO LOAD IN NOMINAL VOLTAGE

Number of turns	*No-load*	*Load 1*	*Load 2*	*Load 3*
0 turn	97.6%	98.0%	97.8%	97.7%
1 turn (2.86%)	97.3%	97.5%	97.6%	97.4%
2 turns (5.71%)	96.4%	96.7%	96.6%	96.5%
3 turns (8.57%)	95.6%	95.9%	95.5%	95.5%
7 turns (20.0%)	90.9%	91.2%	90.2%	89.6%
10 turns (28.57%)	87.1%	87.4%	85.8%	84.5%

healthy operation due to the inherent dynamic eccentricity fault, which causes pole 6 and the neighbouring poles to be smaller than the average value of all the poles. Table II demonstrates that in all load cases, a single short-circuited turn causes a reduction of only 0.2%-0.5% of the faulty pole with respect to the average value of all the poles. This is expected to be far less than the inherent and "natural" variations between the poles. For instance, at maximum load operation with no applied short circuits in the field winding, the average value of is about 1.1% larger than the average value of neighboring pole. It was however hard to determine exactly how much the average value of each pole naturally differed from another pole due to the additional impact of the dynamic eccentricity fault which caused additional variation in average values from one pole to the next. Nevertheless, the measurements confirm that low numbers of short-circuited turns will be hard to detect in a real machine due to the marginal changes.

Fig. 12 depicts the frequency spectrum of the radial flux density obtained from the right sensor at maximum loading conditions. In the simulation results, the frequency spectrum at healthy operation almost exclusively contained the fundamental components and its odd multiples. The impact of the indicated inherent dynamic eccentricity fault of the laboratory generator caused the measured "healthy" spectrum to contain harmonics of substantial magnitude at every multiple of the mechanical frequency.

This caused the fault-related frequency components due to the short-circuited turns to respond quite differently than the results from the finite element analysis. The simulation results showed that inter-turn short circuits would cause the sub-harmonics to experience the largest increase in magnitude and the sub-harmonics responded in a uniform manner for a given number of short-circuited turns. Each of the measured sub-harmonics in Fig. 12 respond quite differently to the short-circuited turns. Some of them increase significantly as a response to the fault, while other increase just slightly.

In the case of 1, 2 and 3 short-circuited turns, some of the sub-harmonics even decreases with increasing fault severity, which is in contradiction to the simulation results. The same goes for the frequency components above the fundamental frequency, which also react differently to the various numbers of shorted turns. For increasing frequency, the harmonics show a diminishing response to the applied faults, in agreement with what the simulation results suggested.

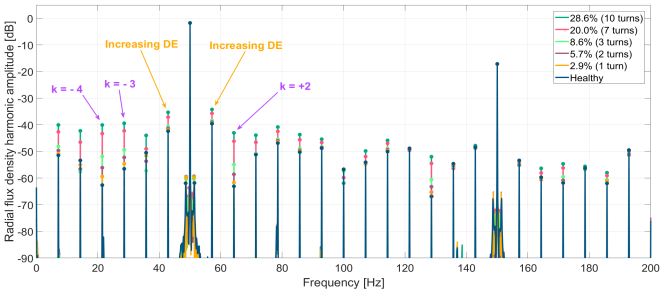

Fig. 12. Spectrum density of the radial flux under short circuit fault in maximum load - Experimental result.

There are a few frequency components that respond as expected to the increasing number of short-circuited turns, for instance the harmonics with k = - 4 an k = 2 which are marked. These components show a consistent increase in amplitude for increasing numbers of short-circuited turns. The harmonics at multiples of the mechanical frequency adjacent to the fundamental frequency (k = 1), were found to be a direct result of dynamic eccentricity. These two components are also the largest components in the measured "healthy" spectra of the experimental result, which further verifies that these components are strongly related to dynamic eccentricity.

VI. Conclusion

In this paper, the inter-turn short circuit fault in the excitation winding of the salient pole synchronous generator based on an air gap magnetic field is studied using the FE approach. Experimental results of the 100 kVA custom made SPSG is used to verify the FE results. The proposed procedure for inter-turn short circuit fault detection is based on using two hall effect sensors in the opposite direction. Comparing the average magnetic field in a polar diagram, the sum of the magnetic field of the two sensors, and the frequency spectrum of them could reveal the fault severity and location. The verified result by the experimental test is as follows: A high number of shorted turns could be detected immediately by analyzing the average magnetic filed distribution or polar diagram. A uniform increase in the amplitude of the lower order harmonic components in the flux density spectrum could be observed. Monitoring the sum of magnetic flux of the two sensors in a machine that only has short circuit fault could be an invaluable tool for diagnostic purposes since the magnitude of the sum of the magnetic flux density spectrum shows better response by increasing the number of shorted turns. The measurement should be coordinated with an encoder in order to identify the location of the faulty pole.

VII. Acknowledgment

The authors gratefully acknowledge the contributions of Vladimir Klubicka, and Morten Flå for their work on the preparation of the experimental test-rig.

References

[1] I. Sadeghi, H. Ehya, J. Faiz, and A. A. S. Akmal, "Online condition monitoring of large synchronous generator under short circuit fault — a review," in *2018 IEEE International Conference on Industrial Technology (ICIT)*, Feb 2018, pp. 1843–1848.

[2] J. Yun, S. Park, C. Yang, Y. Park, S. B. Lee, M. Šašić, and G. C. Stone, "Comprehensive monitoring of field winding short circuits for salient pole synchronous motors," *IEEE Transactions on Energy Conversion*, vol. 34, no. 3, pp. 1686–1694, Sep. 2019.

[3] J. Yun, S. B. Lee, M. Šašić, and G. C. Stone, "Reliable flux-based detection of field winding failures for salient pole synchronous generators," *IEEE Transactions on Energy Conversion*, vol. 34, no. 3, pp. 1715–1718, Sep. 2019.

[4] D. R. Albright, "Interturn short-circuit detector for turbine-generator rotor windings," *IEEE Transactions on Power Apparatus and Systems*, vol. PAS-90, no. 2, pp. 478–483, March 1971.

[5] A. Elez, S. Car, and S. Tvorić, "Air gap magnetic field–key parameter for synchronous and asynchronous machine fault detection," *International Review of Electrical Engineering (IREE)*, vol. 8, no. 3, pp. 1–8, 2013.

[6] O. Kokoko, A. Merkhouf, A. Tounzi, M. Essalhi, E. Guillot, B. Kedjar, and K. Al Haddad, "Detection of short circuits in the rotor field winding in large hydro generator," in *2018 XIII International Conference on Electrical Machines (ICEM)*, Sep. 2018, pp. 1815–1820.

[7] B. Mork, "Comparison measures for benchmarking time domain simulations."

VIII. Biographies

Hossein Ehya (S'19) received the M.Sc. degree in electrical engineering from the Department of Electrical and Computer Engineering, University of Tehran, Tehran, Iran, in 2013. From 2013 to 2018, Ehya worked as a electrical design engineer in electrical machines companies. He is currently working toward the Ph.D. degree in electrical engineering with Norwegian University of Science and Technology (NTNU), Trondheim, Norway. He is working on electromagnetic analysis and fault detection of synchronous machines. His research intrests include signal processing, pattern recognition, design, modeling, and fault diagnosis of electrical machines.

Arne Nysveen (M'98–SM'06) received his Dr.ing. in 1994 from Norwegian Institute of Technology (NTH). From 1995 to 2002 Nysveen worked as a research scientist at ABB Corporate Research in Oslo, Norway. Since 2002 Nysveen has been a professor at the Norwegian University of Science and Technology (NTNU). He is in charge for the turbine and generator technology research in the Norwegian Research Centre for Hydropower Technology (HydroCen).

Ingrid Linnea Groth received the M.Sc. degree in Electric Power Engineering from the Norwegian University of Science and Technology, Trondheim, Norway, in 2019. She is currently with Siemens, Trondheim, Norway.

Bruce A. Mork (SM'08) received the BSME, BSEE,and Ph.D. degrees in Electrical Engineering from North Dakota State University, Fargo, ND, USA, in 1979, 1981, and 1992, respectively. From 1982 to 1986, he was a Design Engineer with the Burns and McDonnell Engineering, Kansas City, MO, USA, in the areas of substation design, protective relaying and control, and communications. He joined the faculty of Michigan Technological University, Houghton, MI, USA, in 1992, where he is now at the rank of Professor.